THE JOURNAL OF PHYSICAL CHEMISTRY C

Article

Cite This: J. Phys. Chem. C 2018, 122, 27148−27155

pubs.acs.org/JPCC

Ultrafast Interfacial Charge Transfer of Cesium Lead Halide Perovskite Films $CsPbX_3$ (X = Cl, Br, I) with Different Halogen Mixing

Pingli Zhang,[†,‡] Gangbei Zhu,[§] Ying Shi,[†,‡] Yunpeng Wang,[∥] Jiahua Zhang,[∥] Luchao Du,*[,†,‡] and Dajun Ding*[,†,‡]

[†]Institute of Atomic and Molecular Physics and [‡]Jilin Provincial Key Laboratory of Applied Atomic and Molecular Spectroscopy, Jilin University, Changchun 130012, China

[§]National Key Laboratory of Shock Wave and Detonation Physics, Institute of Fluid Physics, China Academy of Engineering Physics, Mianyang 621900, China

[∥]State Key Laboratory of Luminescence and Applications, Changchun Institute of Optics, Fine Mechanics and Physics, Chinese Academy of Sciences, Changchun 130033, China

Supporting Information

ABSTRACT: Understanding the interfacial charge transfer of the photoinduced transients of all-inorganic cesium lead halide perovskites ($CsPbX_3$; X = Cl, Br, I) is critical for their photovoltaic applications. Ultrafast dynamics can provide comprehensive information about the transient behavior of the carriers and their transfer mechanism in the materials. In this work, the interfacial charge transfer of $CsPbX_3$ films assembled with TiO_2 with different halogen doping ratios was studied using femtosecond transient absorption spectroscopy combined with global analysis. Four subsequent decay processes after photoexcitation were carried out, including hot carrier cooling, free exciton formation, electron transfer, and charge recombination. The results indicate that the time constant of the interfacial electron transfer varies with the location of the trap state of these perovskites and the relative energy of conduction bands in the perovskite and TiO_2 and that the time constant of the charge recombination can be attributed to the electron−hole interactions. These interpretations are supported by calculations based on first-principles density functional theory. Higher iodine doping in such perovskite $CsPbX_3/TiO_2$ systems increases the time constants of the electron transfer and charge recombination, which suggests that all-inorganic perovskite $CsPbX_3$ with a high iodine content is favorable for improving the power conversion efficiency of solar cells.

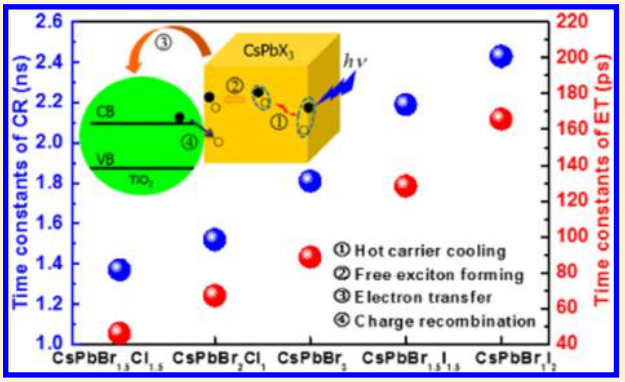

INTRODUCTION

Organic−inorganic methylammonium lead halide ($MAPbX_3$; X = Cl, Br, I) perovskites have recently emerged as one of the most promising candidates for the next generation of solar cell materials.[1−9] In the past five years, the use of these materials as light-absorption layers has greatly improved the power conversion efficiency.[10] $MAPbX_3$ perovskites possess several properties that are suitable for photovoltaic applications such as high carrier mobility, long carrier diffusion length, and suitable optical band gap.[2,3,11] However, despite the gratifying progress in power conversion efficiency, organic−inorganic $MAPbX_3$ perovskites exhibit significant degradation in performance after just a few days of operation.[12,13] New all-inorganic cesium lead halide ($CsPbX_3$; X = Cl, Br, I) perovskites are now considered as potential alternative materials for photovoltaic, laser, and photodetector applications[14−16] because of their potential of tuning the band gap in the visible spectrum, broad spectral absorption, and better stability.[14−17] Although extensive research has been done for the design and development of devices that incorporate these new perovskite materials, the physical processes remain far from clear, especially for the key factors that affect the photoelectric conversion efficiency, such as photoinduced carrier separation, transport, and recombination processes.

The underlying phenomenon responsible for improvement of the solar cell photoelectric conversion efficiency can be clarified on the basis of revealing its microscopic mechanism. Photoelectric conversion is related to the generation of carriers by optical absorption, carrier separation, carrier diffusion, transmission, and collection. This series of processes usually occurs on a time scale of femtoseconds to microseconds and can therefore be experimentally studied by sensitive ultrafast spectroscopic methods. The carrier mobility and carrier recombination lifetime are known to be the key factors

Received: July 27, 2018
Revised: November 4, 2018
Published: November 5, 2018

DOI: 10.1021/acs.jpcc.8b07237
J. Phys. Chem. C 2018, 122, 27148−27155

restricting the photoelectric conversion efficiency of perovskite solar cells. Although the ultrafast dynamics of perovskite materials has been studied and significant attention has been devoted to the study of charge mobility and diffusion,[2,18−20] the physical mechanisms of carrier separation and recombination in these materials remain unclear; thus, further experimental and theoretical studies are needed.

Only a few ultrafast spectroscopic studies for the separation, transport, and recombination of photogenerated carriers in all-inorganic perovskites $CsPbX_3$ have been recently reported.[21−27] Ghosh et al. studied the free carrier recombination in colloidal $CsPbBr_3$ perovskite using time-domain terahertz spectroscopy.[21] They confirmed that the influence of surface defects on trapping the charge carriers is negligible and that this perovskite possesses a remarkably high carrier mobility and a large diffusion length. Han et al. reported two-photon absorption for $CsPbBr_3$ quantum dots (QDs) of different sizes using femtosecond transient absorption (TA) spectroscopy and found that the two-photon absorption cross section is proportional to the linear one-photon absorption and follows a power-law dependence on the size of QDs.[26] Samanta et al. obtained distinct identities of excitons and free charge carriers and distinguished among hot and cold charge carriers in a photoexcited all-inorganic $CsPbBr_xI_{3-x}$ perovskite nanocrystal (NC) system.[22] Recently, a few experiments have focused on the challenge for engineering charge transfer at the interfaces of all-inorganic perovskite materials[28−32] because understanding the charge transfer mechanisms at the interface is one of the major requirements for developing an efficient photovoltaic system. In 2015, Lian et al. first reported the study of interfacial charge transfer dynamics of $CsPbBr_3$ QDs using ultrafast TA spectroscopy,[28] and they found that electron transfer to benzoquinone (BQ) and the subsequent charge recombination occurred with half-lives of ∼65 ps and ∼2.6 ns, respectively, and hole transfer to phenothiazine and the subsequent charge recombination decay had half-lives of ∼49 ps and ∼1 ns, respectively. Bakr et al. investigated the effects of heterovalent doping on carrier dynamics and band structure at the interface of perovskite NCs and molecular acceptors.[29] They used TA spectroscopy to demonstrate that charge transfer at the interface of the NCs can be tuned and promoted by heterovalent doping. It is also found that doping increases the energy difference between the molecular acceptor and the donor moiety and then promotes the interfacial charge transfer process. To enlighten the physical mechanism of carrier transfer, all-inorganic perovskites assembled with titanium dioxide (TiO_2) are taken as an example for further research on the interfacial charge transfer. Herein, we designed the corresponding experimental scheme, synthesized a series of cubic-phase $CsPbX_3$ films with different halide compositions via annealing at high temperature, and assembled them with TiO_2. The ultrafast carrier dynamics of the photoinduced transients of the thus-obtained $CsPbX_3/TiO_2$ films was characterized via femtosecond TA spectroscopy. Global analysis was adopted, which revealed four kinetic components from the TA spectra. Furthermore, first-principles density functional theory (DFT) was used to elucidate the electronic structure of the $CsPbX_3$ perovskite. Compared with the experimental data, the charge carrier (or exciton) dynamics was interpreted using the energy gap and electron density of states (DOSs) based on DFT calculations.

EXPERIMENTAL SECTION

$CsPbX_3$ NCs were synthesized using a previously reported method with some modifications.[33] The perovskite films were deposited via spin-coating $CsPbX_3$ solution on a mesoporous TiO_2/glass substrate. All of the materials were used without further purification. Perovskite films were prepared under nitrogen protection. Finally, we obtained samples with the following compositions: $CsPbBr_{1.5}Cl_{1.5}/TiO_2$, $CsPbBr_2Cl_1/TiO_2$, $CsPbBr_3/TiO_2$, $CsPbBr_{1.5}I_{1.5}/TiO_2$, and $CsPbBr_1I_2/TiO_2$. See the Supporting Information (S1) for the detailed preparation process.

Diffractograms of $CsPbX_3/TiO_2$ perovskite films were recorded through X-ray diffraction (XRD) measurements using a PANalytical Empyrean X-ray diffractometer at a voltage of 40 kV and a current of 40 mA. The scanning angle range was 5−50° (2θ) at a scanning rate of 3°/min.

Steady-state absorption spectra were measured using a UV-3101PC UV−vis−near-infrared scanning spectrophotometer. To further clarify the interfacial charge transfer mechanism of $CsPbX_3/TiO_2$ films, we characterized the ultrafast dynamics of charge carriers by time-resolved TA measurement (Figure 1),

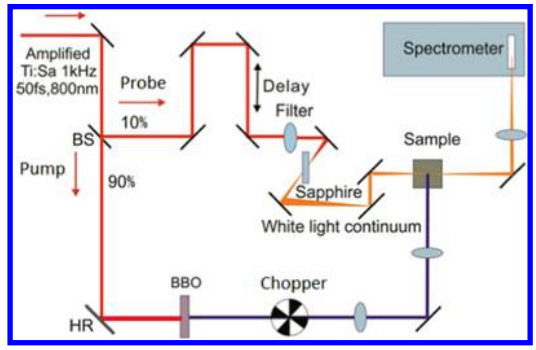

Figure 1. Experimental setup for the time-resolved TA measurements.

as described in a previous study.[34] A Ti:Sapphire laser system (Libra-USP-HE, Coherent Inc.) with a central wavelength of 800 nm, a repetition rate of 1 kHz, and a pulse width of 50 fs was used. The fundamental output of the laser was divided into two beams with an intensity ratio of 9:1. The 90% intensity beam was used for producing a 400 nm pump pulse through a barium boron oxide crystal. The other beam (10% intensity) was focused on a sapphire crystal to generate a white-light continuum from 450 to 800 nm used as a probe pulse through the sample with respect to the pump pulse. A delay stage was used to change the distance of light path of the probe beam and obtain the time delay. The probe beam was focused on the sample surface and overlapped with the pump beam. The optical diameters of the pump and probe beams were ∼2.5 and 1.0 mm, respectively. The energy flux for photoexcitation was attenuated to 2 $\mu J/cm^2$ to avoid any damage to the samples. All of the TA measurements were performed at room temperature.

To further illustrate how the energy gap and electron DOS affect the charge carrier dynamics of the excited states, the first-principles DFT calculation was performed[35−37] beginning from the cubic $CsPbBr_3$ perovskite crystals. Mixed-halide crystal structures were obtained by replacing Br with Cl^- or I^- anions. The structural and electronic properties of the cubic $CsPbX_3$ perovskites were studied using the plane-wave norm-conserving pseudopotential method with an energy cutoff of 820 eV on the basis of DFT with the revised Perdew−Burke−

DOI: 10.1021/acs.jpcc.8b07237
J. Phys. Chem. C 2018, 122, 27148−27155

Ernzerhof exchange−correlation functional of the generalized gradient approximation (GGA-RPBE). The Brillouin-zone integrations were derived using a 2 × 2 × 2 *k*-point set.

RESULTS AND DISCUSSION

Optical Characterization. Figure 2 shows the steady-state absorption spectra of the synthesized $CsPbX_3/TiO_2$ films. The

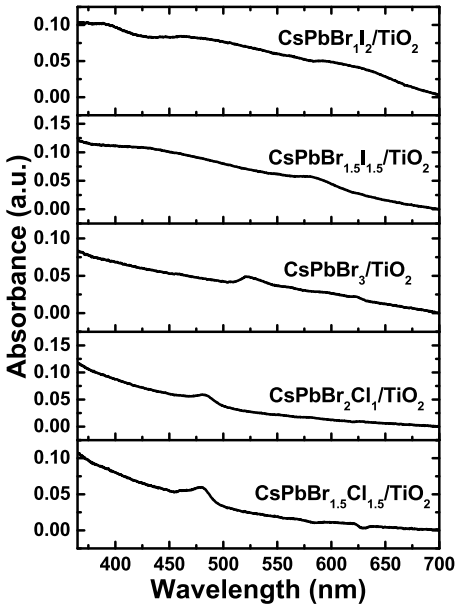

Figure 2. Steady-state absorption spectra of different $CsPbX_3/TiO_2$ films.

$CsPbBr_3/TiO_2$ sample exhibited a peak at 524 nm, which was attributed to the transition from the valence band maximum (VBM) to the conduction band minimum (CBM),[4,38] similar to that of the organic−inorganic $MAPbX_3$ perovskites. This absorption peak was tuned by varying the halogen composition. When Cl^- anions were introduced into the reaction system, the peak showed a blue shift, whereas the introduction of I^- anions caused a red shift, which is consistent with the trend observed in the TA spectra (Figure S5). Therefore, the absorption peak of $CsPbX_3/TiO_2$ perovskites-based materials can be tuned by controlling the type and stoichiometry of the halogen constituent.

The XRD patterns of the $CsPbBr_3/TiO_2$ film showed diffraction peaks at 15.32, 21.58, 30.47, and 37.76°, corresponding to the (100), (110), (200), and (211) crystal planes.[15,16] These peaks could be attributed to the cubic structure of the $CsPbBr_3$ crystal[15,39] (a = 5.97 Å; space group $Pm3m$), as described in the Electronic Properties of Mixed-Halide Perovskites section. The structure of both $CsPbCl_3$ and $CsPbBr_3$ perovskite crystals is either tetragonal or monoclinic at room temperature and translates into a cubic phase at 47 and 130 °C, respectively, whereas that of $CsPbI_3$ one undergoes a similar phase change at 308 °C.[40] In our experiment, the cubic phase was formed due to the annealing of the perovskite films at 450 °C. Based on our calculations, the band gap of the cubic $CsPbBr_3$ perovskite was 2.40 eV. As shown in Figure 3, with increasing Cl^- anions, all of the peaks in the XRD diffractograms shifted to larger angles, whereas the increase of I^- anions shifted them to smaller angles. As the type and ratio of halogens change, the peak positions move only

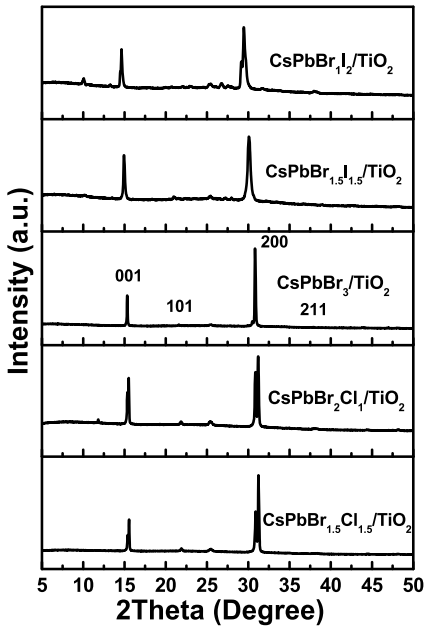

Figure 3. XRD diffractograms of different $CsPbX_3/TiO_2$ films.

slightly and no other diffraction peaks appear. We believe that the halogen mixing and change of the stoichiometry do not change the crystal phase. Hence, the crystal phases of perovskites with different halide components are all cubic (Figure 3).

TA Measurements and Global Analysis of the $CsPbBr_3/TiO_2$ System. To investigate the physical mechanisms of the interfacial charge transfer of the mixed-halide perovskites, the femtosecond TA measurements were performed with 400 nm (photon energy of 3.1 eV) laser excitation. The excitation energy of 2 $\mu J/cm^2$ at the sample was chosen mainly for a better signal-to-noise ratio and to avoid damaging the samples. All of the measurements were performed under the same experimental conditions. As shown in Figure 2, the absorption peak of $CsPbBr_3/TiO_2$ is at 524 nm but that of free $CsPbBr_3$ QDs is at 510 nm, as reported in the literature.[14,39] The shift of the absorption peak indicates an interfacial charge transfer.

Figure 4 shows the TA spectra of $CsPbBr_3/TiO_2$ at different delay times. The TA spectra exhibited the following features: a broad absorption band at around 510 nm (labeled as PA1), a bleaching band ($\Delta OD < 0$, where ΔOD is the change in absorption) at 525 nm (labeled as PB1), and a second absorption band at around 530 nm (labeled PA2). The negative (bleaching) signal is sandwiched between two positive absorption bands; as such, to better understand the physical mechanisms of the interfacial charge transfer of $CsPbX_3/TiO_2$ films, a global analysis of the TA spectra involving multiple wavelengths instead of the single-wavelength kinetic analysis was performed.

The TA spectra of the $CsPbBr_3/TiO_2$ film (Figure 4) were separated into several components by singular value decomposition (SVD).[41,42] SVD combined with global fitting is an effective analytical method for complex spectra with overlapping features. Using this analysis, we expected to extract the main components from the original data, remove the unnecessary components, and then reasonably analyze the extracted principal components to obtain the spectrum and kinetic curves of the transient components and filter out the

DOI: 10.1021/acs.jpcc.8b07237
J. Phys. Chem. C 2018, 122, 27148−27155

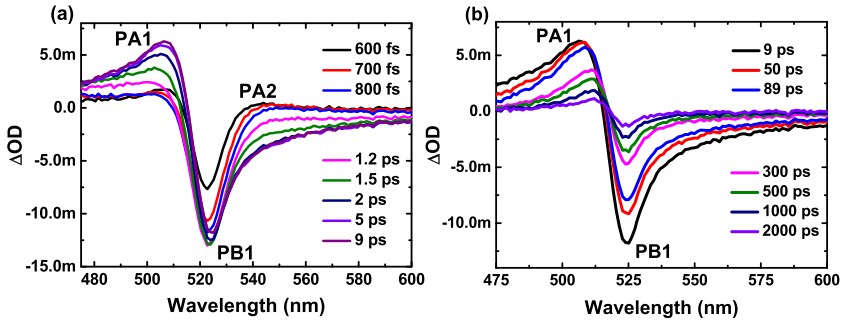

Figure 4. TA spectra of $CsPbBr_3/TiO_2$ on the (a) short (0.6–9 ps) and (b) long (9–2000 ps) time scales upon excitation at 400 nm (1 kHz, 50 fs, 2 $\mu J/cm^2$).

experimental noise. The measured TA data are a two-dimensional matrix A consisting of m_λ wavelengths and n_t times. Any one of the elements in matrix A can be expressed as follows

$$A_{ij} = A(\lambda_i, t_j)$$

For matrix A of real elements, SVD is defined by the product of three matrices, called the SVD of A

$$A = USV^T$$

where the column vectors of U and V are referred to as the left and right singular vectors of A, respectively, S is the singular value of the SVD transient component, and U contains the basis spectra of the data matrix A. The analysis yields four kinetic components: 765 ± 55 fs, 8.89 ± 0.73 ps, 88.69 ± 6.12 ps, and 1.81 ± 0.16 ns, as is evident from the decay-associated spectra (DAS) shown in Figure 5. DAS are decay functions

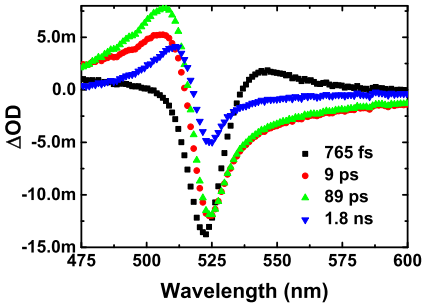

Figure 5. Decay-associated spectra (DAS) of $CsPbBr_3/TiO_2$.

associated with specific time-constant components obtained through our data analysis. The time constants observed in Figure 5 are functions of the entire kinetic system and cannot be associated with any given species.[43] The DAS do not correspond to real spectra observed experimentally; they correspond to real spectra only when a component decays without interconversions to other components. The DAS are interpreted as loss or gain of bleaching or absorption with a certain time constant.

PA1 is reported to be attributed to the absorption arising from the lowest excitonic state,[22] and PA2 is attributed to the absorption due to hot charge carriers (hot excitons) with a delay time of 765 fs.[22−25,44] After 765 fs, the absorption signal of PA2 weakens and is eventually replaced by PB1 signals. We attribute PB1 to the depopulation of the ground state, and its position matches that of the absorption peak of $CsPbBr_3/TiO_2$ in the steady-state absorption spectrum in Figure 2. Our TA results have three spectral features: PA1, PA2, and PB1. Mondal et al. reported four spectral features in TA results for $CsPbBr_3$ NCs without TiO_2: PA1, PA2, PB1, and PB2.[22] The morphology (film or NCs) of the all-inorganic perovskite material does not affect the spectral signatures of the TA measurements.[24] The disappearance of the PB2 signal in our system may be due to the hot carrier (hot exciton) cooling to the lowest excitonic state and transport toward the interface. Our TA spectra (Figure 4a) show that the disappearance of PA2 is accompanied by an increase in the PA1 signal, which reaches the absorption maximum at 9 ps.

The hot carriers (hot excitons) created by the 400 nm excitation are located far above the band edge. Thus, the 765 fs rise profile of the PA2 signal arises from the cooling of these hot carriers (hot excitons) to the band-edge excitonic state. The 9 ps component more likely arises from free exciton formation. Lian et al. reported that the lifetimes of electron transfer and charge recombination for $CsPbBr_3$ QDs are 65 ps and 2.6 ns, respectively.[28] For $CsPbBr_3/TiO_2$, we estimated electron transfer and charge recombination lifetimes of 89 ps and 1.8 ns, respectively, which are comparable with the results of Lian et al. Our results are therefore reasonable. The 89 ps decay observed was due to electron transfer[28,29,32] from the conduction band (CB) of $CsPbBr_3$ to the CB of TiO_2. The energy difference between the CB of $CsPbBr_3$ and the CB of the electron acceptor promotes electron transfer.[29,31] The electron transfer process occurs after the free excitons have dissociated; the electrons will transport and be trapped in the CB of TiO_2 following the electron escape from the trap state and will continue to diffuse in TiO_2. Charge recombination occurs when the electrons diffuse in TiO_2 until they reach the region close to the valence band (VB) of the mixed-halide perovskites. The presence of an 89 ps component indicates that the TiO_2, as an electron acceptor, provides a transport channel for the transfer of photogenerated electrons. The 1.8 ns component is attributed to the charge recombination process[28,29,32] because electrons escape from the trap state of TiO_2 and diffuse back to the CB of TiO_2, where they recombine with a hole in the VB of $CsPbBr_3$, resulting in electron–hole recombination. The energy difference between the CB of TiO_2 and the VB of $CsPbBr_3$ can promote the charge recombination process.[29,31] To gain further physical insight into the mechanism of the interfacial charge transfer between $CsPbBr_3$ and the electron acceptor (TiO_2), we propose a possible interfacial charge transfer path in $CsPbBr_3/TiO_2$, as shown in Figure 6. The trapped state is at the defect of the surface state, where the charge transfer and charge recombination processes occur.

DOI: 10.1021/acs.jpcc.8b07237
J. Phys. Chem. C 2018, 122, 27148−27155

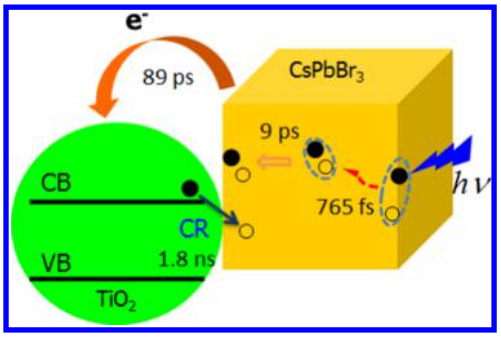

Figure 6. Proposed path for the interfacial charge transfer in the $CsPbBr_3/TiO_2$ system. The black lines are the conduction band (CB) and the valence band (VB), and the blue arrow indicates the charge recombination process.

TA Spectral Character and Interfacial Charge Transfer of Mixed-Halide Perovskites $CsPbX_3/TiO_2$ Systems. The experimental measurements reveal that the obtained spectral features of the mixed-halide perovskite $CsPbX_3/TiO_2$ systems are very similar to those observed for the $CsPbBr_3/TiO_2$ system (Figures 4, 5 and S1–S5). However, the positions of the spectral peaks are closely related to the type/proportion of the halide. For example, compared with that of the PB1 band of pure $CsPbBr_3/TiO_2$, the red shift of the PB1 band increased with increasing iodine content. Because the CB and VB energy levels of $CsPbX_3$ are contributed by lead and halogen, respectively, the band gap is reduced when bromine is replaced by iodine, resulting in a red shift of PB1.[22,27,45] This phenomenon can also be seen in their steady-state spectra, as shown in Figure 2. In the case of chorine substitution, the PB1 band undergoes a blue shift because of an increase in the band gap.

We obtained the time constants of different decay processes for different mixed-halide perovskite $CsPbX_3/TiO_2$ systems using the global fitting from the experimental TA measurements (Table 1). We focused on the interfacial influence on electron transfer and charge recombination in these systems. We found that the time constant for the electron transfer of mixed-halide perovskites $CsPbX_3/TiO_2$ with a higher iodine content is slower than that of $CsPbX_3/TiO_2$ with a higher bromine content (this trend is consistent with Wang's results[32]): 89 ps for $CsPbBr_3$ and 166 ps for $CsPbBr_1I_2$. In contrast, the time constant of $CsPbX_3/TiO_2$ with a higher chlorine content is faster than that of the $CsPbX_3/TiO_2$ with a higher bromine content: 89 ps for $CsPbBr_3$ and 46 ps for $CsPbBr_{1.5}Cl_{1.5}$. Additionally, the time constants for charge recombination gradually increased as the halide composition was changed from chlorine to iodine, e.g., 1.37 ns for $CsPbBr_{1.5}Cl_{1.5}$, 1.81 ns for $CsPbBr_3$, and 2.43 ns for $CsPbBr_1I_2$.

Table 1. Time Constants of the Decay-Associated Spectra of Different $CsPbX_3/TiO_2$ Systems[a]

mixed	hot carrier (hot exciton) cooling (fs)	free exciton formation (ps)	electron transfer (ps)	charge recombination (ns)
$CsPbBr_{1.5}Cl_{1.5}$	471	7.14	46.21	1.37
$CsPbBr_2Cl_1$	450	8.74	67.27	1.52
$CsPbBr_3$	765	8.89	88.69	1.81
$CsPbBr_{1.5}I_{1.5}$	591	11.67	128.37	2.19
$CsPbBr_1I_2$	760	3.66	165.73	2.43
$CsPbBr_3$ NCs[b]	450			
$CsPbBr_3$ NCs[c]	700		45 (CCT)	2.0
$CsPbBr_3$ film[d]	651			
$CsPbBr_3$/BQ[e]			65	2.6
$CsPbI_3$ NCs[f]	560		215 (CCT)	>2.0

[a]CCT: charge carrier trapping. [b]Global fitting results upon 400 nm excitation.[23] [c]Global fitting results upon 350 nm excitation.[22] [d]Single-wavelength fitting results upon 400 nm excitation.[24] [e]Single-wavelength fitting results upon 400 nm excitation.[28] [f]Global fitting results upon 545 nm excitation.[22]

The electron transfer process is affected by the location of the trap states of the perovskite and the relative energy of CBs in the perovskite and TiO_2. First, the trap states in $CsPbCl_3$ are located near the band edge, whereas those in $CsPbI_3$ are closer to the higher excitonic states, which leads to a substantially slower trapping rate of $CsPbI_3$ than that of $CsPbCl_3$.[22] Moreover, the time constant of electron transfer for the mixed Br/Cl perovskite is smaller than that for the mixed Br/I perovskite because the relative energy of the CBs for the mixed Br/Cl perovskite is higher.[45,46]

Diffusion lengths of carriers can affect the time constant of charge recombination.[2,3] Chlorine addition reduces the time constant of electron–hole recombination because of the shorter electron–hole diffusion length in the $CsPbBr_{1.5}Cl_{1.5}$ perovskite. On the other hand, the longer time constant of recombination in the iodine-added perovskite results from a much larger diffusion length of carriers. Furthermore, charge recombination occurs at the localized state of the interface;[47,48] the greater density of holes in the chlorine-added perovskite can enhance the interaction between electrons and holes.

The aforementioned findings suggest that all-inorganic perovskite $CsPbX_3$ with a high iodine content is favorable for application to improve the power conversion efficiency of solar cells.

In addition, the hot carriers (hot excitons) induced in $CsPbBr_3/TiO_2$ by photoexcitation are rapidly cooled at a time scale of 765 fs, which is similar to the result reported by Butkus et al. (651 fs)[24] but longer than that for the relaxation of the hot carriers in colloidal $CsPbBr_3$ perovskite (<450 fs).[23,25] From Table 1, the relaxation time changed from 471 fs for the mixed Br/Cl perovskite to 760 fs for the mixed Br/I perovskite. Such ultrafast hot carrier relaxation is attributed to electron–phonon scattering.[44,49−51] The relaxation rate of the hot carriers (k_{cool}) strongly depends on the electron–phonon coupling factor (S_{HR}); i.e., k_{cool} is directly proportional to S_{HR}.[25] The proportional relationship between S_{HR} and the overlap integral of the electronic states[25] suggests that the relaxation rate of the hot carriers is largely dependent on the halide species and is mainly determined by the DOSs of the $CsPbX_3$ crystals. After hot carrier cooling in the $CsPbBr_3$ perovskite, free excitons are formed within a time constant of 9 ps. This time constant is lower for the mixed Br/Cl perovskite, likely because of faster cooling rates of the hot carriers.[49] For $CsPbBr_1I_2/TiO_2$, the global fitting gives a time constant of 3.66 ps for free exciton formation; the reason for this result is ambiguous at present, although Auger recombination, which occurs in all-inorganic halide perovskites,[21,23] may be involved.

Electronic Properties of Mixed-Halide Perovskites. The effects of halogen mixing on the electronic properties of $CsPbX_3$ perovskites are discussed on the basis of DFT with GGA-RPBE. We calculated the DOSs, band gaps, lattice

DOI: 10.1021/acs.jpcc.8b07237
J. Phys. Chem. C 2018, 122, 27148−27155

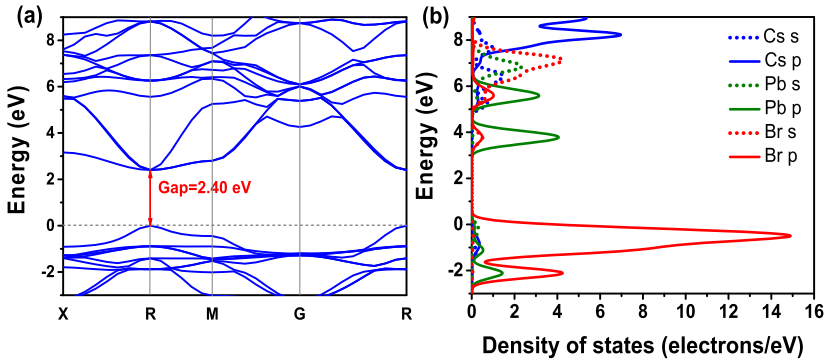

Figure 7. (a) Band structure of the $CsPbBr_3$ crystal. (b) Partial densities of states of the $CsPbBr_3$ crystal.

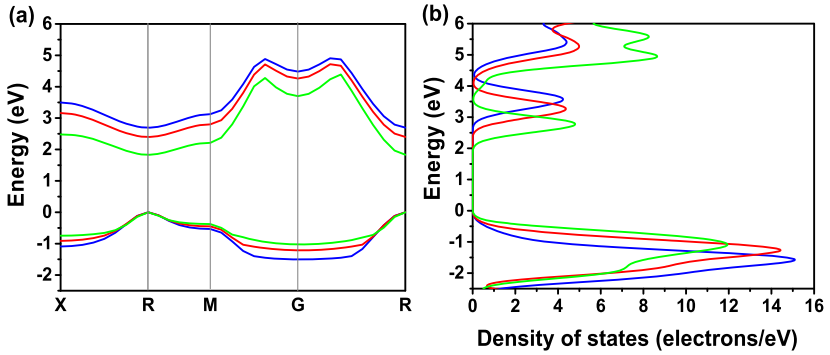

Figure 8. (a) Band structures of the highest VB (VB_1) and the lowest CB (CB_1) for $CsPbX_3$ (X = Cl, Br, I) crystal structures. (b) Densities of states of $CsPbX_3$ (X = Cl, Br, I) crystal structures. Blue, $CsPbCl_3$; red, $CsPbBr_3$; green, $CsPbI_3$.

constants, and unit cell volumes for the various all-inorganic perovskite crystals (the results are provided in Table S1).

For $CsPbBr_3$, as shown in Figure 7, the calculated band gap is 2.40 eV. Its partial density of states (PDOS) shows that the lowest CB (CB_1) mainly formed by the 6p state of Pb and the highest VB (VB_1) is mainly by the 4p state of Br. Thus, the electronic transitions are mainly from the 4p state of Br to the 6p state of Pb so that the excited state is dominated by Pb and Br. PDOS analysis also shows that the contribution of Cs in both VB_1 and CB_1 is significantly lower than that of Br or Pb.

For mixed $CsPbX_3$, the calculations show that because VB and CB are mainly occupied by halogen and lead, the introduction of halogen anions can affect the band gap and DOS of $CsPbX_3$. When X changes from Cl to Br to I, the valence orbital changes from 3p to 4p or 5p, corresponding to a monotonic decrease of the perovskite band gap. The VB_1 and the CB_1 of these three perovskite structures are shown in Figure 8a. For the mixed Br/Cl perovskites, the band gap increases from 2.40 to 2.70 eV when Br is replaced with a suitable proportion of Cl. In contrast, the band gap decreases from 2.40 to 1.83 eV when Br is replaced with I. According to the Fermi golden rule, the transition probability of a mixed Br/Cl perovskite is lower than that of a mixed Br/I perovskite.[37] This trend is similar to that of the experimental observations, supporting the proposed model of charge transfer (Figure 6). The DOSs of these three perovskite structures are shown in Figure 8b, which shows that the bonding types in the molecular orbitals of these three perovskites are substantially the same but their locations and strengths are different. The perovskite with a higher chlorine content has a stronger ion binding energy than that with a higher iodine content, which indicates that the structure of mixed Br/Cl perovskite is more stable than that of mixed Br/I perovskite.

CONCLUSIONS

Ultrafast spectroscopic measurements combined with first-principles DFT calculations have been performed for exploring the interfacial charge transfer mechanism of different mixed-halide cesium lead halide perovskite films $CsPbX_3$ (X = Cl, Br, I) assembled with TiO_2 systems. Different time constants for several decays were obtained from a global analysis, which were assigned to hot carrier cooling, free exciton formation, electron transfer, and charge recombination in these systems. From these data, we suggest a charge transfer model to explain the ultrafast interfacial charge transfer mechanism of $CsPbX_3/TiO_2$ with different X compositions. We found that doping of more I content in such $CsPbX_3$ perovskite materials can increase the time constant of the electron transfer and charge recombination. Therefore, we speculate that $CsPbX_3$ with a high iodine content and assembled with TiO_2 is a promising candidate for improving the efficiency of solar cell photoelectric conversion. Our results provide dynamic information about controlling the electron transfer and charge recombination processes at the interface of these promising all-inorganic perovskite materials.

ASSOCIATED CONTENT

Supporting Information

The Supporting Information is available free of charge on the ACS Publications website at DOI: 10.1021/acs.jpcc.8b07237.

Sample preparation, decay-associated spectra of $CsPbX_3/TiO_2$, femtosecond TA spectra at a 20 ps delay for different $CsPbX_3/TiO_2$ films, structural

DOI: 10.1021/acs.jpcc.8b07237
J. Phys. Chem. C 2018, 122, 27148−27155

parameters, and band gaps of different $CsPbX_3$ crystal structures (PDF)

AUTHOR INFORMATION

Corresponding Authors

*E-mail: lcdu@jlu.edu.cn (L.D.).
*E-mail: dajund@jlu.edu.cn (D.D.).

ORCID

Pingli Zhang: 0000-0002-6354-8781

Author Contributions

P.Z. carried out the experiment and performed the theoretical calculation. L.D. gave the idea of our investigation. Y.W. executed sample preparation. J.Z., Y.S., and G.Z. provide the technical support. D.D. provided the investigation guidance and helpful discussion.

Notes

The authors declare no competing financial interest.

ACKNOWLEDGMENTS

This work is supported by the Natural Science Foundation of China (grants 11674125 and 21003155), the Key project of the National Natural Science Foundation of China (grant 20933010), and Jilin Provincial Department of Education Program (JJKH20170777KJ).

REFERENCES

(1) Zhu, Z.; Ma, J.; Wang, Z.; Mu, C.; Fan, Z.; Du, L.; Bai, Y.; Fan, L.; Yan, H.; Phillips, D. L.; et al. Efficiency Enhancement of Perovskite Solar Cells through Fast Electron Extraction: The Role of Graphene Quantum Dots. *J. Am. Chem. Soc.* **2014**, *136*, 3760−3763.

(2) Xing, G.; Mathews, N.; Sun, S.; Lim, S. S.; Lam, Y. M.; Gräetzel, M.; Mhaisalkar, S.; Sum, T. C. Long-Range Balanced Electron- and Hole-Transport Lengths in Organic-Inorganic $CH_3NH_3PbI_3$. *Science* **2013**, *342*, 344−347.

(3) Stranks, S. D.; Eperon, G. E.; Grancini, G.; Menelaou, C.; Alcocer, M. J. P.; Leijtens, T.; Herz, L. M.; Petrozza, A.; Snaith, H. J. Electron-Hole Diffusion Lengths Exceeding 1 Micrometer in an Organometal Trihalide Perovskite Absorber. *Science* **2013**, *342*, 341−344.

(4) Stamplecoskie, K. G.; Manser, J. S.; Kamat, P. V. Dual Nature of the Excited State in Organic-Inorganic Lead Halide Perovskites. *Energy Environ. Sci.* **2015**, *8*, 208−215.

(5) Sheng, C.; Zhang, C.; Zhai, Y.; Mielczarek, K.; Wang, W.; Ma, W.; Zakhidov, A.; Vardeny, Z. V. Exciton Versus Free Carrier Photogeneration in Organometal Trihalide Perovskites Probed by Broadband Ultrafast Polarization Memory Dynamics. *Phys. Rev. Lett.* **2015**, *114*, No. 116601.

(6) Marchioro, A.; Teuscher, J.; Friedrich, D.; Kunst, M.; van de Krol, R.; Moehl, T.; Graetzel, M.; Moser, J.-E. Unravelling the Mechanism of Photoinduced Charge Transfer Processes in Lead Iodide Perovskite Solar Cells. *Nat. Photonics* **2014**, *8*, 250−255.

(7) Zhou, H.; Chen, Q.; Li, G.; Luo, S.; Song, T.-b.; Duan, H.-S.; Hong, Z.; You, J.; Liu, Y.; Yang, Y. Interface Engineering of Highly Efficient Perovskite Solar Cells. *Science* **2014**, *345*, 542−546.

(8) Liu, M.; Johnston, M. B.; Snaith, H. J. Efficient Planar Heterojunction Perovskite Solar Cells by Vapour Deposition. *Nature* **2013**, *501*, 395−398.

(9) Heo, J. H.; Im, S. H.; Noh, J. H.; Mandal, T. N.; Lim, C.-S.; Chang, J. A.; Lee, Y. H.; Kim, H.-j.; Sarkar, A.; Nazeeruddin, M. K.; et al. Efficient Inorganic−Organic Hybrid Heterojunction Solar Cells Containing Perovskite Compound and Polymeric Hole Conductors. *Nat. Photonics* **2013**, *7*, 486−491.

(10) See https://www.nrel.gov/pv/assets/pdfs/pv-efficiencies-07-17-2018.pdf for NREL chart.

(11) Wehrenfennig, C.; Liu, M.; Snaith, H. J.; Johnston, M. B.; Herz, L. M. Charge-Carrier Dynamics in Vapour-Deposited Films of the Organolead Halide Perovskite $CH_3NH_3PbI_{3-x}Cl_x$. *Energy Environ. Sci.* **2014**, *7*, 2269−2275.

(12) Noh, J. H.; Im, S. H.; Heo, J. H.; Mandal, T. N.; Seok, S. I. Chemical Management for Colorful, Efficient, and Stable Inorganic−Organic Hybrid Nanostructured Solar Cells. *Nano Lett.* **2013**, *13*, 1764−1769.

(13) Christians, J. A.; Miranda Herrera, P. A.; Kamat, P. V. Transformation of the Excited State and Photovoltaic Efficiency of $CH_3NH_3PbI_3$ Perovskite Upon Controlled Exposure to Humidified Air. *J. Am. Chem. Soc.* **2015**, *137*, 1530−1538.

(14) Protesescu, L.; Yakunin, S.; Bodnarchuk, M. I.; Krieg, F.; Caputo, R.; Hendon, C. H.; Yang, R. X.; Walsh, A.; Kovalenko, M. V. Nanocrystals of Cesium Lead Halide Perovskites ($CsPbX_3$, X = Cl, Br, and I): Novel Optoelectronic Materials Showing Bright Emission with Wide Color Gamut. *Nano Lett.* **2015**, *15*, 3692−3696.

(15) Wang, Y.; Li, X.; Song, J.; Xiao, L.; Zeng, H.; Sun, H. All-Inorganic Colloidal Perovskite Quantum Dots: A New Class of Lasing Materials with Favorable Characteristics. *Adv. Mater.* **2015**, *27*, 7101−7108.

(16) Song, J.; Li, J.; Li, X.; Xu, L.; Dong, Y.; Zeng, H. Quantum Dot Light-Emitting Diodes Based on Inorganic Perovskite Cesium Lead Halides ($CsPbX_3$). *Adv. Mater.* **2015**, *27*, 7162−7167.

(17) Akkerman, Q. A.; D'Innocenzo, V.; Accornero, S.; Scarpellini, A.; Petrozza, A.; Prato, M.; Manna, L. Tuning the Optical Properties of Cesium Lead Halide Perovskite Nanocrystals by Anion Exchange Reactions. *J. Am. Chem. Soc.* **2015**, *137*, 10276−10281.

(18) Kim, H.-S.; Lee, C.-R.; Im, J.-H.; Lee, K.-B.; Moehl, T.; Marchioro, A.; Moon, S.-J.; Humphry-Baker, R.; Yum, J.-H.; Moser, J. E.; et al. Lead Iodide Perovskite Sensitized All-Solid-State Submicron Thin Film Mesoscopic Solar Cell with Efficiency Exceeding 9%. *Sci. Rep.* **2012**, *2*, No. 591.

(19) Lee, M. M.; Teuscher, J.; Miyasaka, T.; Murakami, T. N.; Snaith, H. J. Efficient Hybrid Solar Cells Based on Meso-Superstructured Organometal Halide Perovskites. *Science* **2012**, *338*, 643−647.

(20) Abrusci, A.; Stranks, S. D.; Docampo, P.; Yip, H.-L.; Jen, A. K.-Y.; Snaith, H. J. High-Performance Perovskite-Polymer Hybrid Solar Cells Via Electronic Coupling with Fullerene Monolayers. *Nano Lett.* **2013**, *13*, 3124−3128.

(21) Yettapu, G. R.; Talukdar, D.; Sarkar, S.; Swarnkar, A.; Nag, A.; Ghosh, P.; Mandal, P. Terahertz Conductivity within Colloidal $CsPbBr_3$ Perovskite Nanocrystals: Remarkably High Carrier Mobilities and Large Diffusion Lengths. *Nano Lett.* **2016**, *16*, 4838−4848.

(22) Mondal, N.; Samanta, A. Complete Ultrafast Charge Carrier Dynamics in Photo-Excited All-Inorganic Perovskite Nanocrystals ($CsPbX_3$). *Nanoscale* **2017**, *9*, 1878−1885.

(23) Aneesh, J.; Swarnkar, A.; Ravi, V. K.; Sharma, R.; Nag, A.; Adarsht, K. V. Ultrafast Exciton Dynamics in Colloidal $CsPbBr_3$ Perovskite Nanocrystals: Biexciton Effect and Auger Recombination. *J. Phys. Chem. C* **2017**, *121*, 4734−4739.

(24) Butkus, J.; Vashishtha, P.; Chen, K.; Gallaher, J. K.; Prasad, S. K. K.; Metin, D. Z.; Laufersky, G.; Gaston, N.; Halpert, J. E.; Hodgkiss, J. M. The Evolution of Quantum Confinement in Cspbbr3 Perovskite Nanocrystals. *Chem. Mater.* **2017**, *29*, 3644−3652.

(25) Chung, H.; Jung, S. I.; Kim, H. J.; Cha, W.; Sim, E.; Kim, D.; Koh, W.-K.; Kim, J. Composition-Dependent Hot Carrier Relaxation Dynamics in Cesium Lead Halide ($CsPbX_3$, X = Br and I) Perovskite Nanocrystals. *Angew. Chem., Int. Ed.* **2017**, *56*, 4160−4164.

(26) Chen, J.; Zídek, K.; Chábera, P.; Liu, D.; Cheng, P.; Nuuttila, L.; Al-Marri, M. J.; Lehtivuori, H.; Messing, M. E.; Han, K.; et al. Size- and Wavelength-Dependent Two-Photon Absorption Cross-Section of CsPbBr3 Perovskite Quantum Dots. *J. Phys. Chem. Lett.* **2017**, *8*, 2316−2321.

(27) Hoffman, J. B.; Schleper, A. L.; Kamat, P. V. Transformation of Sintered $CsPbBr_3$ Nanocrystals to Cubic $CsPbI_3$ and Gradient $CsPbBr_xI_{3-x}$ through Halide Exchange. *J. Am. Chem. Soc.* **2016**, *138*, 8603−8611.

DOI: 10.1021/acs.jpcc.8b07237
J. Phys. Chem. C 2018, 122, 27148−27155

(28) Wu, K.; Liang, G.; Shang, Q.; Ren, Y.; Kong, D.; Lian, T. Ultrafast Interfacial Electron and Hole Transfer from $CsPbBr_3$ Perovskite Quantum Dots. *J. Am. Chem. Soc.* **2015**, *137*, 12792−12795.
(29) Begum, R.; Parida, M. R.; Abdelhady, A. L.; Murali, B.; Alyami, N. M.; Ahmed, G. H.; Hedhili, M. N.; Bakr, O. M.; Mohammed, O. F. Engineering Interfacial Charge Transfer in $CsPbBr_3$ Perovskite Nanocrystals by Heterovalent Doping. *J. Am. Chem. Soc.* **2017**, *139*, 731−737.
(30) Sarkar, S.; Ravi, V. K.; Banerjee, S.; Yettapu, G. R.; Markad, G. B.; Nag, A.; Mandal, P. Terahertz Spectroscopic Probe of Hot Electron and Hole Transfer from Colloidal $CsPbBr_3$ Perovskite Nanocrystals. *Nano Lett.* **2017**, *17*, 5402−5407.
(31) Li, H.; Zheng, X.; Liu, Y.; Zhang, Z.; Jiang, T. Ultrafast Interfacial Energy Transfer and Interlayer Excitons in the Monolayer $WS_2/CsPbBr_3$ Quantum Dot Heterostructure. *Nanoscale* **2018**, *10*, 1650−1659.
(32) Zhang, Y.-X.; Wang, H.-Y.; Zhang, Z.-Y.; Zhang, Y.; Sun, C.; Yue, Y.-Y.; Wang, L.; Chen, Q.-D.; Sun, H.-B. Photoluminescence Quenching of Inorganic Cesium Lead Halides Perovskite Quantum Dots ($CsPbX_3$) by Electron/Hole Acceptor. *Phys. Chem. Chem. Phys.* **2017**, *19*, 1920−1926.
(33) Li, X.; Wu, Y.; Zhang, S.; Cai, B.; Gu, Y.; Song, J.; Zeng, H. $CsPbX_3$ quantum Dots for Lighting and Displays: Room-Temperature Synthesis, Photoluminescence Superiorities, Underlying Origins and White Light-Emitting Diodes. *Adv. Funct. Mater.* **2016**, *26*, 2435−2445.
(34) Yin, H.; Li, H.; Xia, G.; Ruan, C.; Shi, Y.; Wang, H.; Jin, M.; Ding, D. A Novel Non-Fluorescent Excited State Intramolecular Proton Transfer Phenomenon Induced by Intramolecular Hydrogen Bonds: An Experimental and Theoretical Investigation. *Sci. Rep.* **2016**, *6*, No. 19774.
(35) Wang, Y.; Gould, T.; Dobson, J. F.; Zhang, H.; Yang, H.; Yao, X.; Zhao, H. Density Functional Theory Analysis of Structural and Electronic Properties of Orthorhombic Perovskite $CH_3NH_3PbI_3$. *Phys. Chem. Chem. Phys.* **2014**, *16*, 1424−1429.
(36) Mosconi, E.; Amat, A.; Nazeeruddin, M. K.; Grätzel, M.; De Angelis, F. First-Principles Modeling of Mixed Halide Organometal Perovskites for Photovoltaic Applications. *J. Phys. Chem. C* **2013**, *117*, 13902−13913.
(37) Feng, J.; Xiao, B. Crystal Structures, Optical Properties, and Effective Mass Tensors of $CH_3NH_3PbX_3$ (X = I and Br) Phases Predicted from HSE06. *J. Phys. Chem. Lett.* **2014**, *5*, 1278−1282.
(38) Manser, J. S.; Kamat, P. V. Band Filling with Free Charge Carriers in Organonietal Halide Perovskites. *Nat. Photonics* **2014**, *8*, 737−743.
(39) Nedelcu, G.; Protesescu, L.; Yakunin, S.; Bodnarchuk, M. I.; Grotevent, M. J.; Kovalenko, M. V. Fast Anion-Exchange in Highly Luminescent Nanocrystals of Cesium Lead Halide Perovskites ($CsPbX_3$, X = Cl, Br, I). *Nano Lett.* **2015**, *15*, 5635−5640.
(40) Møller, C. K. Crystal Structure and Photoconductivity of Cæsium Plumbohalides. *Nature* **1958**, *182*, 1436.
(41) Henry, E. R.; Hofrichter, J. Singular Value Decomposition: Application to Analysis of Experimental Data. In *Methods in Enzymology*; Academic Press: New York, 1992; Vol. *210*, pp 129−192.
(42) Mei, J.; Wang, F.; Wang, Y.; Tian, C.; Liu, H.; Zhao, D. Energy Transfer Assisted Solvent Effects on $CsPbBr_3$ Quantum Dots. *J. Mater. Chem. C* **2017**, *5*, 11076−11082.
(43) Beechem, J. M.; Ameloot, M.; Brand, L. Global and Target Analysis of Complex Decay Phenomena. *Instrum. Sci. Technol.* **1985**, *14*, 379−402.
(44) Shen, Q.; Ripolles, T. S.; Even, J.; Ogomi, Y.; Nishinaka, K.; Izuishi, T.; Nakazawa, N.; Zhang, Y.; Ding, C.; Liu, F.; et al. Slow Hot Carrier Cooling in Cesium Lead Iodide Perovskites. *Appl. Phys. Lett.* **2017**, *111*, No. 153903.
(45) Ravi, V. K.; Markad, G. B.; Nag, A. Band Edge Energies and Excitonic Transition Probabilities of Colloidal $CsPbX_3$ (X = Cl, Br, I) Perovskite Nanocrystals. *ACS Energy Lett.* **2016**, *1*, 665−671.
(46) Mondal, N.; De, A.; Samanta, A. All-Inorganic Perovskite Nanocrystal Assisted Extraction of Hot Electrons and Biexcitons from Photoexcited Cdte Quantum Dots. *Nanoscale* **2018**, *10*, 639−645.
(47) Du, L.; Weng, Y. Photoinduced Charge Recombination at Dye-Sensitized Individual TiO_2 Nanoparticles and Its Application in Probe for the Local Polarity Change around the Nanoparticle in Solution. *J. Phys. Chem. C* **2007**, *111*, 4567−4577.
(48) Du, L.; Furube, A.; Yamamoto, K.; Hara, K.; Katoh, R.; Tachiya, M. Plasmon-Induced Charge Separation and Recombination Dynamics in Gold-TiO_2 Nanoparticle Systems: Dependence on TiO_2 Particle Size. *J. Phys. Chem. C* **2009**, *113*, 6454−6462.
(49) Nah, S.; Spokoyny, B. M.; Soe, C. M. M.; Stoumpos, C. C.; Kanatzidis, M. G.; Harel, E. Ultrafast Imaging of Carrier Cooling in Metal Halide Perovskite Thin Films. *Nano Lett.* **2018**, *18*, 1044−1048.
(50) Fu, J.; Xu, Q.; Han, G.; Wu, B.; Huan, C. H. A.; Leek, M. L.; Sum, T. C. Hot Carrier Cooling Mechanisms in Halide Perovskites. *Nat. Commun.* **2017**, *8*, No. 1300.
(51) Deng, X.; Wen, X.; Huang, S.; Sheng, R.; Harada, T.; Kee, T. W.; Green, M.; Ho-Baillie, A. Ultrafast Carrier Dynamics in Methylammonium Lead Bromide Perovskite. *J. Phys. Chem. C* **2016**, *120*, 2542−2547.

DOI: 10.1021/acs.jpcc.8b07237
J. Phys. Chem. C 2018, 122, 27148−27155